JP Journal of Heat and Mass Transfer

https://pphmjopenaccess.com
https://doi.org/10.17654/0973576324022
Volume 37, Number 3, 2024, Pages 313-328 **P-ISSN: 0973-5763**

EXPLORING ENERGY EFFICIENCY: ASSESSING MECHANICAL AND THERMAL PROPERTIES OF SINTERED FLY ASH AND CLAY-BASED COMPOSITES

Hajar Sdira[1,4], Laila Farissi[2], Houda SOULAMI[1], Mohammed Ali Arbaoui[3], Mohamed Waqif[2], Asmae Arbaoui[1], Latifa Saadi[2], Mouhaydine Tlemçani[4] and Amal Bouich[5]

[1]Thermodynamic Energy Laboratory (LTE)
Faculty of Sciences
Mohammed V University
1014 Rabat, Morocco

[2]Laboratory of Innovative Materials,
Energy and Sustainable Development (IMED-Lab)
Faculty of Science and Technology of Marrakesh
Cadi Ayyad University
549, Marrakech, Morocco

[3]Design and Systems Laboratory (Electronics, Signals and IT) (LCS)
Faculty of Sciences
Mohammed V University
1014 Rabat, Morocco

Received: February 4, 2024; Accepted: April 18, 2024
Keywords and phrases: clay, fly ash, sintering, mechanical and physical properties.

How to cite this article: Hajar Sdira, Laila Farissi, Houda SOULAMI, Mohammed Ali Arbaoui, Mohamed Waqif, Asmae Arbaoui, Latifa Saadi, Mouhaydine Tlemçani and Amal Bouich, Exploring energy efficiency: assessing mechanical and thermal properties of sintered fly ash and clay-based composites, JP Journal of Heat and Mass Transfer 37(3) (2024), 313-328. https://doi.org/10.17654/0973576324022

Published Online: June 3, 2024

[4]Department of Informatics
School of Sciences and Technology
University of Évora
7004-516 Évora, Portugal

[5]Institut de Disseny per a la Fabricació i Producció Automatitzada
Universitat Politècnica de València
46022 Valencia, Spain

Abstract

This study systematically investigates the influence of sintering on the physical and mechanical attributes of clay, both in its pristine state and when blended with varying proportions of fly ash. Employing a diverse array of analytical techniques, encompassing compression tests, measurements of density, porosity, and volume shrinkage, our inquiry seeks to provide a comprehensive elucidation of the alterations and transformations induced by the sintering process, particularly in conjunction with the integration of fly ash.

The analysis discerns a noteworthy correlation between escalating sintering temperatures and the augmentation of key mechanical properties. Specifically, an elevation in Young's modulus, compressive stress, density, and volume shrinkage is evident as the sintering temperature increases. Simultaneously, a consistent diminution in porosity is observed, indicating a complex interplay of factors influencing the material characteristics. The elucidation of these intricate relationships contributes significantly to an advanced understanding of the synergistic effects arising from the combined influence of sintering and fly ash incorporation on the physical and mechanical attributes of the composite material. The implications of this investigation extend to diverse applications in material science and engineering, where a precise comprehension of sintering dynamics is paramount for optimizing the performance of clay-based composites.

1. Introduction

The field of geotechnical engineering has witnessed a surge in research dedicated to the development and evaluation of alternative technologies aimed at enhancing soil behavior. Within the realm of geotechnical engineering, the strategic manipulation of soil characteristics stands as a crucial element in advancing soil stabilization techniques, a historical mainstay in diverse projects ranging from dams and pavements to retaining walls [1, 2]. Among the myriad strategies employed to elevate soil qualities, the utilization of waste materials such as bottom ash, lime, and fly ash for chemical stabilization has surfaced as a particularly promising avenue.

A pressing global concern revolves around the increasing demand for energy and the consequential rise in the generation of fly ash as a byproduct of coal combustion in traditional power plants. This surge in solid waste production necessitates comprehensive environmental protection measures, as exemplified by India, which annually produces a staggering, 120-150 million tons of coal fly ash generated from 120 existing coal based thermal power plants of fly ash alongside an equivalent quantity of Portland cement [3-5]. The composition of fly ash and bottom ash encompasses crucial elements/compounds such as potassium (K), silica (SiO_2), sulfur (S), alumina (Al), calcium (Ca), sulfur (S), sodium (Na), iron oxide (Fe_2O_3), and magnesium (Mg) [6-8].

Recognizing the environmental challenges posed by the escalating volumes of fly ash and bottom ash, research institutions are increasingly exploring their utilization for geotechnical purposes. Incorporating fly ash into soils, particularly those with high and low plasticity, has gained widespread acceptance as an effective technique for improving engineering behavior. Studies indicate that the addition of fly ash to clay-based soils enhances the strength parameters and permeability thereby surpassing the performance of untreated clay specimens [9, 10].

The successful integration of fly ash into clay soil hinges upon an array of factors, wherein the influence of additional ingredients plays a pivotal

role. Notably, the enhancement in unconfined compressive strength achieved through the incorporation of fly ash aligns comparably with other additives such as lime, dust, and sand. A separate facet of this complex scenario unfolds in pavement subgrade construction, where the introduction of lime manifests notable improvements in California Bearing Ratio values [11]. The complexity inherent in optimizing composite mixtures is underscored by the discernible alterations observed in key parameters, including California Bearing Ratio values, optimum moisture content, and maximum dry density, when utilizing construction waste such as ceramic tiles [12-14].

The enhanced bearing capacity associated with the use of fly ash is attributed primarily to its pozzolanic behavior, as indicated by the CaO/SiO_2 ratio and CaO in fly ash [15]. The compressive strength of Fiber Concrete (FC) exhibited a noteworthy enhancement, reaching a peak improvement of 38%, while concurrently experiencing a discernible reduction in thermal conductivity by upto 3.4%. The amelioration in Foamed Concrete's performance was predominantly attributed to the mechanisms of filling, pozzolanic activity, and the enhancement of slurry fluidity facilitated by the incorporation of fly ash [16, 17]. Prudent consideration of the fly ash proportion within the composite mixture is imperative. Excessive quantities of fly ash warrant careful scrutiny, as they have the potential to induce a reduction in shear resistance. Conversely, an elevated concentration of bottom ash emerges as a viable strategy, demonstrating an augmentative effect on the overall strength of the mixture.

Controversy exists regarding the impact of fly ash on soil plasticity and swelling potential, with some studies reporting reductions in plasticity, while others contradict this finding [18]. Furthermore, fly ash serves as a versatile additive, compatible with sand, free lime, geopolymers, slag, dust, bentonite, and gypsum. Noteworthy research efforts have sought to comprehensively evaluate the influence of these additives on soil stabilization, revealing nuanced effects on Atterberg limits, free swell index (FSI), CBR, and UCS [19, 20].

This study contributes to the evolving body of research on fly ash in soil stabilization by focusing on their influence on mechanical and physical parameters. The findings emphasize that the judicious utilization of fly ash waste not only enhances clay's mechanical properties but also facilitates the recycling of thermal power plant's waste. The subsequent sections undertake a comprehensive investigation into the nuanced effects of the sintering process and the incorporation of varying proportions of fly ash on the mechanical and physical properties of clay, thereby offering significant insights pertinent to applications in geotechnical engineering.

2. Materials and Methods

2.1. Samples sources

The various samples were produced from starting materials, red clayey soil (Arg.b) taken from the Demnate site, located near the city of Marrakech and industrial waste, fly ash (CV) produced at the Jorf Lasfar located in the city of El Jadida.

2.2. Preparation of test samples

To prepare the samples, 3 to 4 drops of the Rhodoviol solution were introduced into a mass ranging from 3g to 4g for each formulation. The mixture was then shaped into cylindrical forms using a hydraulic press. The resulting cylindrical test pieces measured $10\text{cm} \times 1.3\text{cm}$. Subsequently, the pellets underwent drying at 100°C for 24 hours, followed by sintering at various temperatures: 900°C, 1000°C, 1100°C and 1150°C, with a heating rate of 1°C/min, over a two-hour period. The heat treatment was conducted in a Carbolite RHF 1500°C electric muffle furnace.

For the mechanical tests, three specimens were prepared for each mixture at every sintering temperature. Table 1 shows the mass percent composition of the prepared formulations.

Table 1. Mass percent composition of the prepared formulations

Formulations/component	Mass percent of mixtures component %	
	Arg.b	C.V
Clay (Arg.b)	100	-
Fly ash (C.V)	-	100
$ArgCV_5$	50	50
$ArgCV_9$	10	90
$ArgCV_7$	30	70

2.3. Characterization techniques

Various experimental techniques were applied to the raw, calcined, and sintered powder samples.

Mechanical compression tests were performed on cylindrical specimens using an Instron-type machine controlled by a computer.

Volumetric calculations were determined by subtracting the final volume (after sintering) from the original volume (before sintering). Bulk density measurements of sintered specimens were obtained using the electronic densimeter H300-S.

The absorbed water test on the sintered specimens was conducted through hydrostatic weighing, employing the formula in equation (1), where m_1 is the mass of the sample before immersion in water and m_2 is the mass after immersion in water for 24 hours.

Equation.

$$\%\text{water absorption} = 100(m_2 - m_1)/m_2. \quad (1)$$

3. Results and Discussion

3.1. Mechanical and physical characterizations of $ArgCV_{i=5,7,9}$ and Arg.b specimens

3.1.1. Effect of sintering temperature on mechanical properties

To investigate the mechanical properties, compression tests were conducted on $ArgCV_{i=5,7,9}$ formulations, as well as on Arg.b specimens sintered at temperatures of 900°C, 1000°C, 1100°C, and 1150°C. The stress-strain curves for these various samples are presented in Figures 1-4. Notably, the curves exhibit a linear relationship between stress and strain before reaching the elastic limit, after which brittle fracture occurs, particularly pronounced at 1100°C. This behavior mirrors observations in ceramic materials [21].

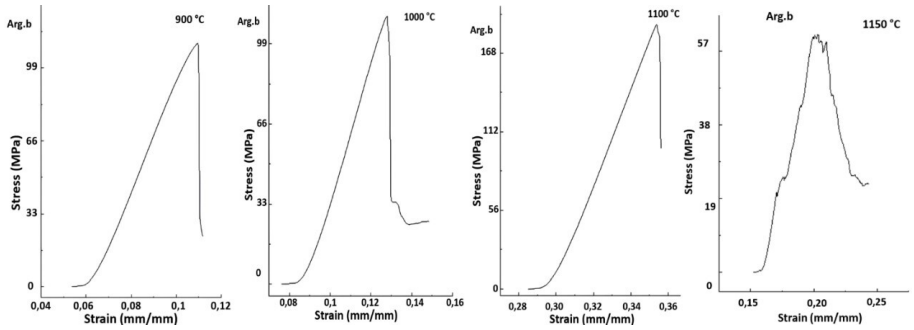

Figure 1. Stress curves as a function of strain of Arg.b.

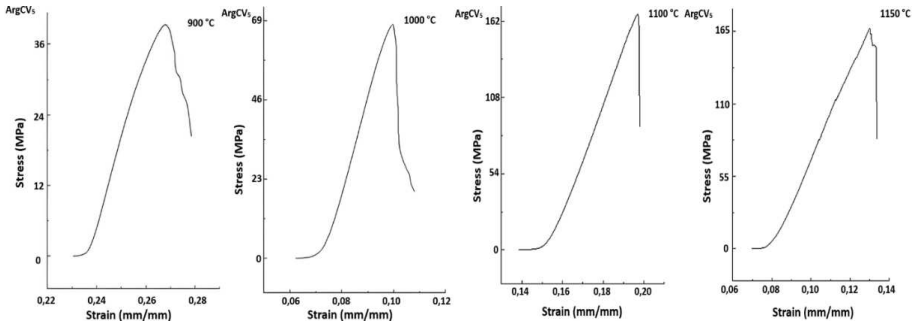

Figure 2. Stress curves as a function of strain of $ArgCV_5$.

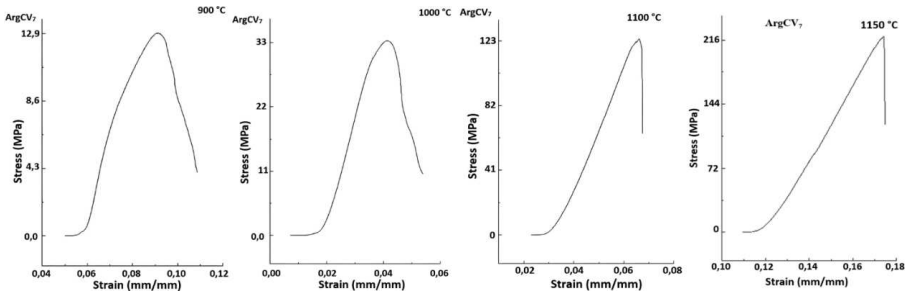

Figure 3. Stress curves as a function of strain of $ArgCV_7$.

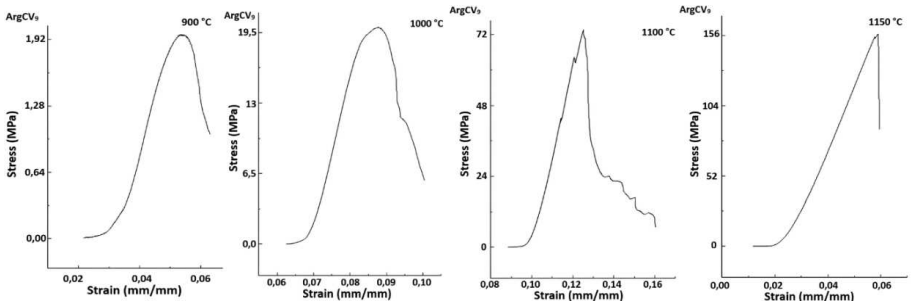

Figure 4. Stress curves as a function of strain of $ArgCV_9$.

Figure 5 consolidates the variation of Young's modulus with respect to the sintering temperature, highlighting that an increase in the fly ash percentage in the mixture leads to a rise in Young's modulus, peaking at 1100°C for all formulations. The $ArgCV_5$ formulation demonstrates the highest Young's modulus value. Additionally, Figure 6 illustrates the curves depicting the variation of compressive stress concerning the sintering temperature. The data suggests that an elevation in the sintering temperature for formulations $(ArgCV_{i=5,7,9})$ corresponds to an increase in compressive stress. However, at 900°C and 1000°C, Arg.b exhibits higher compressive stress values compared to other formulations within the same temperature range. Conversely, at 1150°C, the $ArgCV_7$ formulation records the highest compressive stress, followed by $ArgCV_5$ and $ArgCV_9$. Consequently, the

formulation with the optimal combination of mechanical properties, namely, Young's modulus and compressive stress is identified as $ArgCV_5$ sintered at 1100°C.

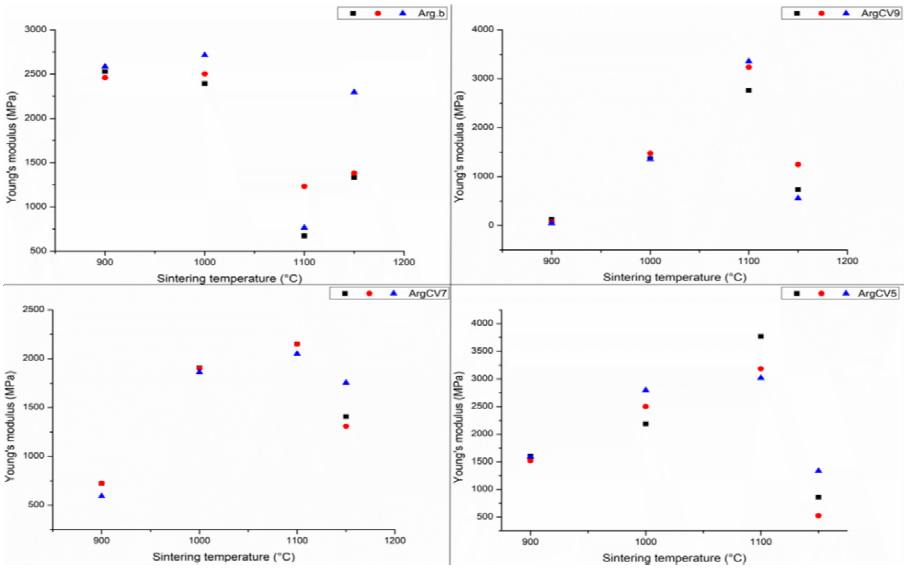

Figure 5. Variation of Young's modulus as a function of the sintering temperature: Arg.b, $ArgCV_9$, $ArgCV_7$ and $ArgCV_5$.

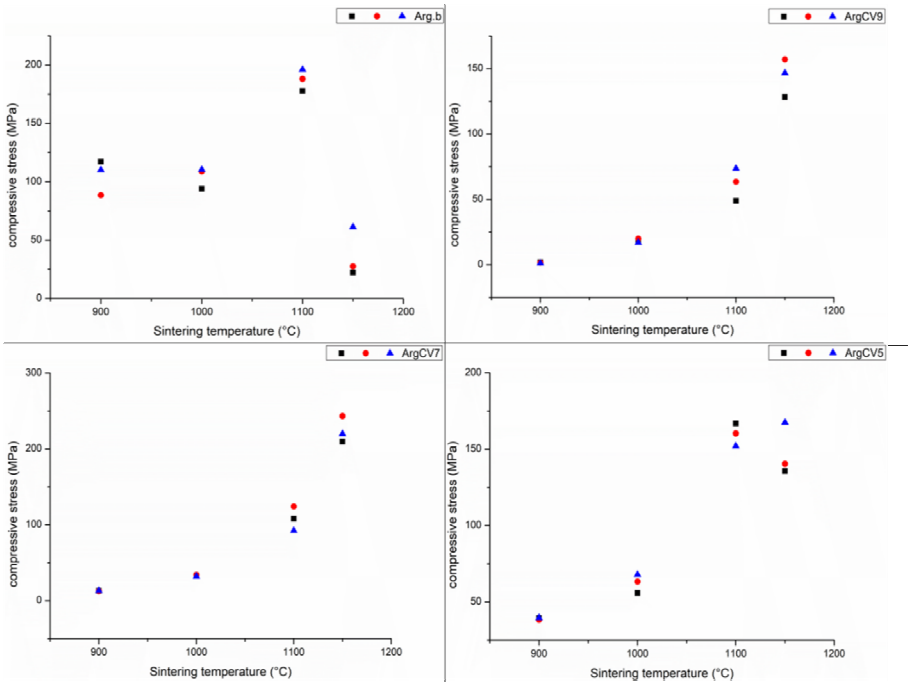

Figure 6. Variation of compressive stress as a function of the sintering temperature: Arg.b, $ArgCV_9$, $ArgCV_7$ and $ArgCV_5$.

3.1.2. Effect of sintering temperature on density

Figure 7 illustrates the variation in density as a function of sintering temperature. Notably, the density of Arg.b samples exhibits a decrease with the increasing sintering temperature until it reaches its minimum at 1150°C. Among the Arg.b samples, those sintered at 900°C, 1000°C, and 1100°C demonstrate the highest density, while the sample sintered at 1150°C is the least dense among all samples derived from the various mixtures.

Excluding the Arg.b samples, those from the $ArgCV_9$ formulation consistently exhibit the lowest density, regardless of their respective sintering temperatures. The $ArgCV_5$ and $ArgCV_7$ samples sintered at 900°C, 1000°C, and 1100°C exhibit a similar trend, where their density decreases at 1000°C and increases at 1100°C. In this sintering temperature

range, $ArgCV_5$ is denser than $ArgCV_7$. However, at 1150°C, the density of $ArgCV_7$ increases, while that of $ArgCV_5$ decreases, resulting in $ArgCV_7$ being denser than $ArgCV_5$ at this temperature.

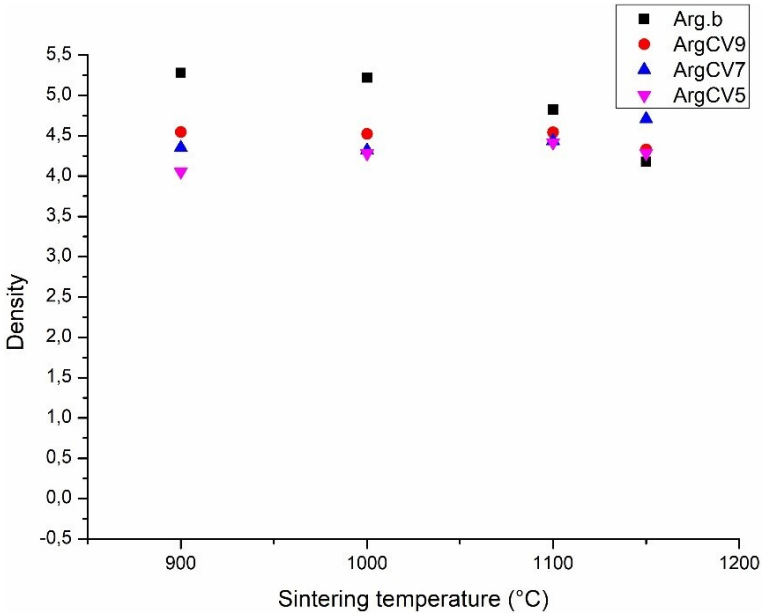

Figure 7. Density variation at different sintering temperatures.

3.1.3. Effect of sintering temperature on porosity

Figure 8 depicts the variation in porosity (water absorption) as a function of the sintering temperature. The results reveal a consistent reduction in porosity for all formulations as the sintering temperature increases. This graph can be delineated into two distinct temperature ranges: $T = \{900°C, 1000°C\}$ and $T = \{1100°C, 1150°C\}$.

In the $T = \{900°C, 1000°C\}$ range, porosity decreases proportionally with the percentage of fly ash in the mixtures/formulations. Contrastingly, in the $T = \{1100°C, 1150°C\}$ range, the porosity behavior shifts, with notable changes observed only in $ArgCV_5$ and Arg.b: The porosity of $ArgCV_5$ diminishes while that of Arg.b increases. Consequently, Arg.b exhibits

higher porosity than $ArgCV_5$. Notably, at 1150°C, water absorption values are closely aligned for all formulations.

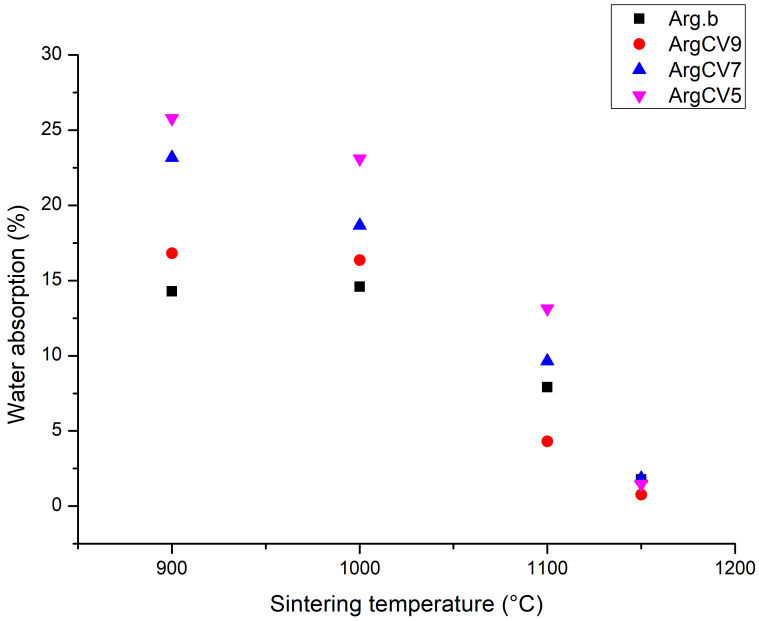

Figure 8. Water absorption variation for different sintering temperatures.

3.1.4. Effect of sintering temperature on volume shrinkage

Figure 9 illustrates the variation in volume shrinkage as a function of the sintering temperature. For formulations $ArgCV_{i=5,7,9}$, the volume shrinkage increases with both the rising sintering temperature and the percentage of fly ash within the formulations. Similarly, Arg.b exhibits volume shrinkage patterns aligned with the sintering temperature and the proportion of fly ash upto 1100°C, where it peaks, followed by a decrease at 1150°C.

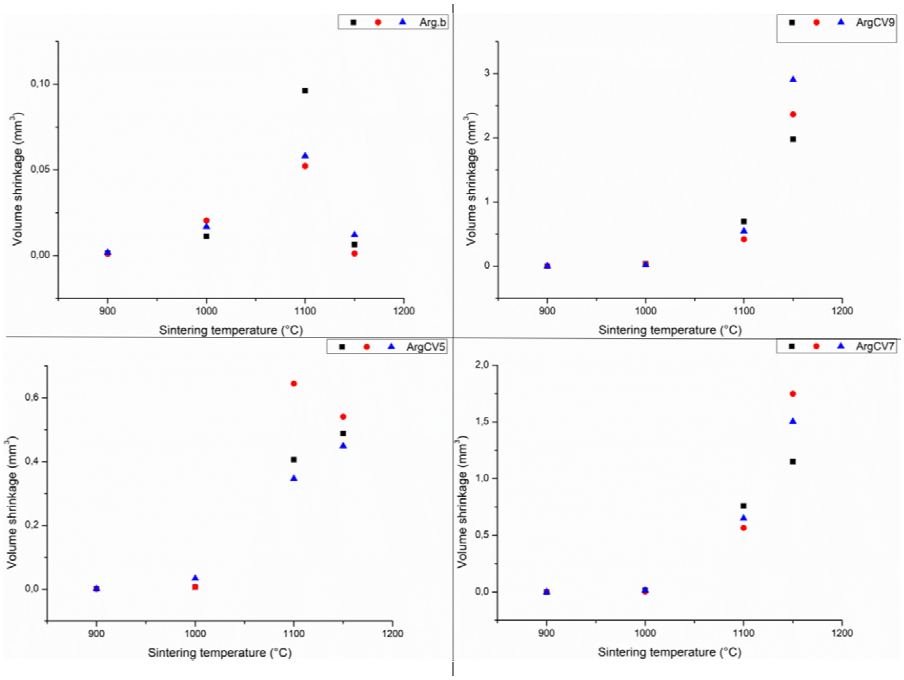

Figure 9. Volume shrinkage variation at different sintering temperatures: Arg.b, $ArgCV_9$, $ArgCV_7$, $ArgCV_5$.

4. Conclusion

In summary, this investigation significantly contributes to the progression of refractory material formulations with the overarching objective of augmenting their mechanical characteristics. The empirical inquiry focused on the sintering, physical and mechanical characterizations of the raw material clay (Arg.b) and its formulations with distinct percentages of fly ash, denoted as $ArgCV_9$, $ArgCV_7$, and $ArgCV_5$.

The intricate relationship between mineralogical composition, the proportion of fly ash, and sintering temperature emerged as pivotal factors exerting a notable influence on the observed physical and mechanical properties. Mechanical assessments underscored the highest compressive

strength in the specimen derived from the $ArgCV_7$ formulation sintered at 1150°C, followed closely by $ArgCV_5$. Remarkably, the $ArgCV_5$ formulation sintered at 1100°C yielded the specimen with the highest Young's modulus, indicative of optimal mechanical attributes.

Density variations were discerned, with Arg.b exhibiting maximal density at 900°C, 1000°C, and 1100°C, while becoming the least dense at 1150°C. Intriguingly, the $ArgCV_7$ specimen manifested the highest density at this elevated temperature. The introduction of fly ash resulted in a reduction of density. Additionally, fly ash incorporation into clay led to an augmentation in water absorption, while escalating sintering temperatures exhibited a converse effect, decreasing water absorption. The least porous specimen emanated from the $ArgCV_5$ formulation sintered at 1150°C. Moreover, volume shrinkage exhibited an upward trend with elevated sintering temperatures and increased fly ash proportions, with the $ArgCV_9$ formulation sintered at 1150°C displaying the maximum volume shrinkage.

In summation, this research elucidates the complex interdependencies among composition, sintering conditions, and resultant mechanical properties, thereby providing invaluable insights for the judicious optimization of formulations tailored to thermal insulation applications in the realm of refractory materials.

References

[1] G. P. Makusa, Soil stabilization methods and materials in engineering practice: state of the art review, Luleå Tekniska Universitet, 2013, pp. 1-35.

[2] M. F. Noaman, M. A. Khan, K. Ali and A. Hassan, A review on the effect of fly ash on the geotechnical properties and stability of soil, Cleaner Mater. 6 (2022), 100151. https://doi.org/10.1016/J.CLEMA.2022.100151.

[3] A. Dwivedi and M. K. Jain, Fly ash-waste management and overview: a review, Recent Research in Science and Technology 6(1) (2014), 30-35.

[4] S. K. Sahu, R. C. Bhangare, P. Y. Ajmal, S. Sharma, G. G. Pandit and V. D. Puranil, Characterization and quantification of persistent organic pollutants in fly ash from coal fueled thermal power stations in India, Journal of Microchemical 92 (2009), 92-96.

[5] B. Lokeshappa and A. K. Dikshit, Disposal and management of coal fly ash, Proc. ICLST, 2011, pp. 11-14.

[6] Debasree Saha et al., Cd, Cr, Co, Pb, and Cu metals in surface and groundwater adjacent to a thermal power plant in Eastern India, Environmental Earth Sciences 81 (2022), Article number 31. https://doi.org/10.1007/s12665-021-10148-0.

[7] Natalia Moreno et al., Physico-chemical characteristics of European pulverized coal combustion fly ashes, Fuel 84 (2005), 1351-1363. https://doi.org/10.1016/j.fuel.2004.06.038.

[8] N. Vig, S. Mor and K. Ravindra, The multiple value characteristics of fly ash from Indian coal thermal power plants: a review, Environmental Monitoring and Assessment 195(1) (2023), 33. doi:10.1007/s10661-022-10473-2.

[9] C. Turan, A. A. Javadi and R. Vinai, Effects of class C and class F fly ash on mechanical and microstructural behavior of clay soil - a comparative study, Materials 15 (2022), 1845.

[10] M. Faisal Noaman, M. A. Khan, K. Ali and A. Jamal, Effect of fly ash on the shear strength of clay soil, Materials Today: Proceedings (2023). https://doi.org/10.1016/j.matpr.2023.02.06.

[11] C. H. Liu and C. Hung, Reutilization of solid wastes to improve the hydromechanical and mechanical behaviors of soils-a state-of-the-art review, Sustain Environ Res. 33 (2023), 17.

[12] A. Sharma, Strength prediction of construction demolition waste and pine needle fibre stabilized soil using artificial neural network, Multiscale and Multidiscip. Model. Exp. and Des. (2023). https://doi.org/10.1007/s41939-023-00304-3.

[13] K. Devi, A. Chhachhia and A. Kumar, Soil improvement using waste materials: a review, Journal of Building Material Science 2(1) (2020), 11-17.

[14] I. Chmielewska and W. Gosk, Safety engineering of anthropogenic objects, No 3 (2022), 34-41. https://doi.org/10.37105/iboa.148.

[15] B. D. Nath, Md. K. A. Molla and G. Sarkar, Study on strength behavior of organic soil stabilized with fly ash, International Scholarly Research Notices (2017), 1-6. https://doi.org/10.1155/2017/5786541.

[16] G. Xian, Z. Liu, Z. Wang and X. Zhou, Study on the performance and mechanisms of high-performance foamed concrete, Materials 15(22) (2022), 7894. https://doi.org/10.3390/ma15227894.

[17] R. Abuelgasim, A. S. A. Rashid, M. Bouassida, N. Shien and M. H. Abdullah, Geotechnical characteristics of Tanjung Bin coal bottom ash, IOP Conf. Ser. Mater. Sci. Eng. 932 (2020), 012055. https://doi.org/10.1088/1757-899X/932/1/012055.

[18] B. Cetin and L. Li, Waste minimization and reuse technologies, M. Kutz, ed., Handbook of Environmental Engineering, 2018. https://doi.org/10.1002/9781119304418.ch20.

[19] A. G. Workie and S. Alam, Effect of lime and fly ash on load bearing capacity of expansive clay soil, International Journal of Innovative Technology and Exploring Engineering 8(11) (2019), 554-563. https://doi.org/10.35940/ijitee.K1573.0881119.

[20] Y. Aslan Topcuoglu and Z. Gurocak, Changes in the strength of high-plasticity clays after stabilization: an experimental study, Iran J. Sci. Technol. Trans. Civ. Eng. 47 (2023), 1109-1123. https://doi.org/10.1007/s40996-022-00991-x.

[21] Yaxun Liu, Lisheng Liu, Hai Mei, Qiwen Liu and Xin Lai, A modified rate-dependent peridynamic model with rotation effect for dynamic mechanical behavior of ceramic materials, Comput. Methods Appl. Mech. Engrg. 388 (2022), 114246. https://doi.org/10.1016/j.cma.2021.114246.